Engineering Journal issn: 0125-8281

*Article*

# Synthesis of Light Hydrocarbons via Oxidative Coupling of Methane over Silica-supported $Na_2WO_4$-$TiO_2$ Catalyst

**Anusorn Seubsai[1,2,3], Palida Tiencharoenwong[1], Phattaradit Kidamorn[1], and Chalida Niamnuy[1,3,*]**

1 Department of Chemical Engineering, Faculty of Engineering, Kasetsart University, Bangkok 10900, Thailand
2 Center of Excellence on Petrochemical and Materials Technology, Kasetsart University, Bangkok 10900, Thailand
3 Research Network of NANOTEC–KU on NanoCatalysts and NanoMaterials for Sustainable Energy and Environment, Kasetsart University, Bangkok 10900, Thailand
*E-mail: fengcdni@ku.ac.th (Corresponding author)

**Abstract.** Methane is of great interest for conversion into high-value hydrocarbons ($C_{2+}$) and olefins, via oxidative coupling of methane (OCM) using catalysts. In this work, $Na_2WO_4$-$TiO_2$/$SiO_2$ catalyst, along with the single catalysts of its components ($Na_2WO_4$/$SiO_2$ and $TiO_2$/$SiO_2$), was investigated for OCM reaction to $C_{2+}$. We found that 5 wt% $Na_2WO_4$+ 5 wt% $TiO_2$ on the $SiO_2$ support was a superior catalyst for OCM reaction compared to the single catalysts. The maximum $C_{2+}$ formation of the $Na_2WO_4$-$TiO_2$/$SiO_2$ catalyst was found under test conditions of a $N_2$/($4CH_4$:$1O_2$) feed gas ratio of 1:1, a reactor temperature of 700 ºC, and gas hourly space velocity of 9,500 $h^{-1}$, exhibiting 71.7% $C_{2+}$ selectivity, 6.8% $CH_4$ conversion, and 4.9% $C_{2+}$ yield. Moreover, the activity of the catalyst had good stability over 24 h of on-stream testing. The characterizations of the $Na_2WO_4$-$TiO_2$/$SiO_2$ catalyst using XRD, FT-IR, XPS, FE-SEM, and TEM revealed that a crystalline structure of α-cristobalite of $SiO_2$ was present along with $TiO_2$ crystals, substantially enhancing the activity of the catalyst for OCM reaction to $C_{2+}$.

**Keywords:** Catalyst, light hydrocarbons, oxidative coupling of methane, sodium tungsten oxide, titanium oxide.

**ENGINEERING JOURNAL** Volume 23 Issue 5
Received 28 March 2019
Accepted 10 June 2019
Published 30 September 2019
Online at http://www.engj.org/
DOI:10.4186/ej.2019.23.5.169

*This article is based on the presentation at The 8th International Thai Institute of Chemical Engineering and Applied Science Conference (ITIChE2018) in Chonburi, Thailand, 8th-9th November 2018.*

DOI:10.4186/ej.2019.23.5.169

## 1. Introduction

Methane ($CH_4$) is the main compound of biogas and natural gas that are plentiful on Earth. It is considered a greenhouse gas with an environmental impact more than 25 times greater than $CO_2$ if equal amounts of these two gases are released into the atmosphere. Since methane is an abundant compound on Earth, a process that can convert methane to high value-added chemicals is a highly attractive topic for many researchers. One of the challenging topics to be considered in catalysis is oxidative coupling of methane (OCM)—a gas-phase reaction that uses $O_2$ or air to directly react with $CH_4$ to produce useful hydrocarbons ($C_{2+}$) such as ethylene, ethane, propane, and propylene [1, 2]. The OCM reaction is an exothermic reaction in nature and normally takes place at reaction temperatures of 600–1,000 ºC [3]. OCM can produce CO and $CO_2$ as byproducts. However, if a suitable catalyst is present, the reaction produces a selective product and extreme reaction temperatures can be reduced.

In the past several years, some potential catalysts have been reported, including $MnO_x$ modified with different types of co-catalysts, supports and promotors, such as oxides of Mg, Na, and Ce. However, the $C_{2+}$ yields and $C_{2+}$ selectivities were quite low at approximately <16% and 25-78%, respectively [4-8]. Additionally, coke formation was found during the reaction, resulting in catalyst deactivation. Later, the coking formation was, however, prevented by introducing of chlorinated compounds with the reactant gases. Alternatively, a binary catalyst of $Na_2WO_4$-$MnO_x$ has been widely investigated because this metal combination was identified as an active material for the OCM reaction. The modified $Na_2WO_4$-$MnO_x$ catalysts reported include $MO_x$-$Na_2WO_4$-$MnO_x$/$SiO_2$ (M = Ni, Co, Fe, Li, Al, Ba, Ca, Na, and K) [9], $TiO_2$-$Na_2WO_4$/$MnO_x$/$SiO_2$ [10], and $Ce_2O_3$-$MnO_x$-$Na_2WO_4$/$SiO_2$ [7]. The $C_{2+}$ yields and $C_{2+}$ selectivities of those $Na_2WO_4$-$MnO_x$ catalysts increased compared to the single catalysts of its component and the other metal combinations due to synergistic catalyst effects between $Na_2WO_4$ and $MnO_x$ [11-14]. The additions of the promoters (e.g. $TiO_2$, $Ce_2O_3$) onto the $Na_2WO_4$-$MnO_x$ catalysts resulted in improved activity of the catalysts, because the promoters could cooperate into the catalytic materials and/or the number of suitable strong basic sites increased [15, 16]. Normally, $SiO_2$ is used as a catalyst support because the $SiO_2$ support is stable under the test conditions and inert to the products [14].

Since previous results reported in the literatures showed that any catalysts containing $Na_2WO_4$, $MnO_x$, and/or $SiO_2$ are highly active for OCM reaction, it is of great interest and challenging to improve new catalysts that consist of any of those components and new active metal component (i.e co-active metal, promoter). In a catalyst screening for OCM reaction in our laboratory, we discovered that addition of $TiO_2$ onto the $Na_2WO_4$/$SiO_2$ catalyst without $MnO_x$ can also substantially improve the $C_{2+}$ yield. This combination of $TiO_2$ and $Na_2WO_4$ on $SiO_2$ has never been reported in detail. Herein, we report on various studies on the activity of $Na_2WO_4$ mixed with $TiO_2$ on $SiO_2$ support. The studies include catalyst optimization, catalyst stability, operating condition for the reaction, and catalyst characterization.

## 2. Experimental Section

### 2.1. Catalyst Preparation

All of the catalysts were synthesized using co-impregnation of predetermined weights of $SiO_2$ as follows. An aqueous solution of $Na_2WO_4$ (sodium tungstate dihydrate, 98.0~101.0%, Daejung) and $Ti^{4+}$(titanium (IV) isopropoxide, 97+%, Alfa Aesar) in ethanol (99.9%, QREC) were determined and pipetted into amorphous fume silica ($SiO_2$, surface area of 85-115 $m^2/g$, Alfa Aesar) to obtain a desired weight percentage of the metal components ($TiO_2$ and/or $Na_2WO_4$) on the $SiO_2$ support. Note that the weight percentage of $TiO_2$ or $Na_2WO_4$ on the support was determined on the basis of the mass of Ti(0) or $Na_2WO_4$, respectively. The mixture was continuously stirred at 120 ºC until dry. The obtained powder was then taken to calcine in an air furnace at 800 ºC for 4 h. After the calcination, a fine white powder was obtained.

### 2.2. Catalyst Activity Test

The activities of the prepared catalysts were evaluated for OCM reaction in a plug flow reactor at 1 atm and a reactor temperature range of 600–800 ºC. A sample (8 mg) was packed in a quartz tubular reactor that had an inner diameter of 0.5 cm. The catalyst bed length was approximately 2 mm and the catalyst was

sandwiched between two layers of quartz wool. The feed gas consisted of nitrogen ($N_2$, 99.999% purity, Praxair), methane ($CH_4$, 99.999% purity, Praxair), and oxygen ($O_2$, 99.999% purity, Praxair) at a volume ratio of ($N_2$:$CH_4$:$O_2$) = (0–7.5):4:1 (i.e. fixing the volume ratio of $CH_4$:$O_2$ = 4:1) with a total feed flow rate of 50 mL/min, which corresponded to a gas hourly space velocity (GHSV) of 9,500 $h^{-1}$. The effluent gas was analysed using a gas chromatograph (Shimadzu, GC-14A) equipped with a thermal conductivity detector (TCD; for analyzing CO, $CO_2$, and $CH_4$) and a flame ionization detector (FID; for analysis of $C_2H_4$, $C_2H_6$, $C_3H_6$, $C_3H_8$ and $C_4H_8$, and $C_4H_{10}$). The catalytic activities are expressed in terms of %$CH_4$ conversion, %$C_{2+}$ selectivity, %$CO_x$ selectivity, and %$C_{2+}$ yield, which are shown in Eq. (1)–(4). The data were collected after the system had reached the set point for 2h.

$$\%\ CH_4\ \text{conversion} = \frac{\text{moles of } CH_4 \text{ input} - \text{moles of } CH_4 \text{output}}{\text{moles of } CH_4 \text{ input}} \times 100 \quad (1)$$

$$\%\ C_{2+}\ \text{selectivity} = \frac{\text{moles of } C_{2+}}{\text{Total moles of products}} \times 100 \quad (2)$$

$$\%\ CO_x\ \text{selectivity} = \frac{\text{moles of } CO_x}{\text{Total moles of products}} \times 100 \quad (3)$$

$$\%\ C_{2+}\ \text{yield} = \frac{\%\ CH_4\text{conversion} \times \%\ C_{2+}\text{selectivity}}{100} \quad (4)$$

### 2.3. Catalyst Characterization

The patterns of powder X-ray diffraction (XRD) the samples were received using a powder X-ray diffractometer (PXRD; X-Pert, Philips and JDX-3530, JEOL) with using Cu-$K_a$ radiation with 40 mA and 45 kV, 0.5 s step time, 0.02° step size.

The pore volumes, pore-sizes, and specific surface areas of the samples were evaluated using $N_2$-physisorption with a Quantachrome Autosorp-1C instrument and Brunauer-Emmett-Teller (BET) procedure at a temperature of −196 °C.

The surface morphology of the samples was imaged using a field emission scanning electron microscope (FE-SEM, JSM7600F, JEOL) with an energy dispersive X-ray spectrometer (EDS), operated at 300 kV). Each sample was coated by gold (Au) using Au sputtering technique.

The particles at the nano-scale of the catalysts were characterized using a high-resolution transmission electron microscope (HR-TEM, JEM-3100F, JEOL) performed at 300 kV.

The Fourier-transform infrared (FT-IR) patterns of the samples were acquired using an FT-IR spectrometer (TENSOR2, Bruker, attenuated total reflection (ATR) mode). For the measurements, fine powder of each catalyst was mixed with potassium bromide (KBr), and then made into a KBr pellet.

The electronic states of sodium, tungsten, and titanium were analyzed using X-ray photoelectron spectroscope (XPS, Axis Ultra DLD, Kratos) with Al Kα for the X-ray source.

The metal-support and metal-metal interactions were analyzed using the $H_2$-temperature programmed reduction ($H_2$-TPR) technique. The $H_2$-TPR profiles of the samples were attained by carrying out the measurements in a tubular reactor (Inconel tube) in a temperature range of 50–900 °C with a heating rate of 5 °C/min. A gas mixture of 9.6% $H_2$ in Ar at a total feed flow rate of 30 mL/min was introduced into the sample bed. A TCD-equipped gas chromatography (GC-14, Shimadzu) was used to continuously monitor the $H_2$ consumption.

## 3. Results and Discussion

### 3.1. Activity of $TiO_2/SiO_2$, $Na_2WO_4/SiO_2$, and $TiO_2$-$Na_2WO_4/SiO_2$ Catalysts

The 10wt% $TiO_2/SiO_2$, 10wt% $Na_2WO_4/SiO_2$, and (5wt% $TiO_2$-5wt% $Na_2WO_4$)/$SiO_2$ catalysts were prepared and tested for OCM reaction, as presented in Fig. 1. The performance of each catalyst was described using the $C_{2+}$ selectivity, $CH_4$ conversion, and $C_{2+}$ yield. It should be noted that the $C_{2+}$ yield is the criterion used to identify a superior catalyst when comparing the activities of catalysts. The $C_{2+}$ yield of

the $Na_2WO_4$-$TiO_2/SiO_2$ catalyst was obtained at 2.7 %, clearly greater than that of the single $TiO_2/SiO_2$ or $Na_2WO_4/SiO_2$ catalysts, approximately 1.5 or 3.8 times the $C_{2+}$ yield of the $TiO_2/SiO_2$ or $Na_2WO_4/SiO_2$ catalysts, respectively. However, the $C_{2+}$ selectivity for these three catalysts was similar (approximately 39–42%) but the $CH_4$ conversion of the $TiO_2/SiO_2$ and $Na_2WO_4/SiO_2$ catalysts was lower than that of the $Na_2WO_4$-$TiO_2/SiO_2$ catalyst. The results indicated that the combination of $TiO_2$ and $Na_2WO_4$ on the $SiO_2$ support reveals a synergistic catalysis effect.

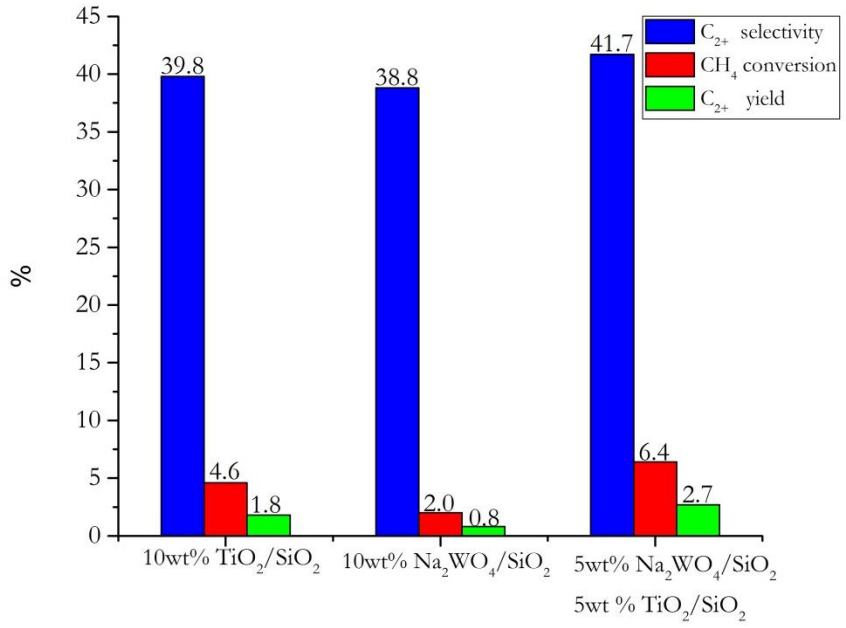


Fig. 1. $C_{2+}$ selectivity, $CH_4$ conversion, and $C_{2+}$ yield of 10wt% $TiO_2/SiO_2$, 10wt% $Na_2WO_4/SiO_2$, and $TiO_2$-$Na_2WO_4/SiO_2$ catalysts. Testing conditions: feeding gas ratio of $CH_4$:$O_2$ = 4:1 by volume, total feed flow rate = 50 mL/min (GHSV = 9,500 $h^{-1}$), and reactor temperature = 700 °C.

### 3.2. Effect of $TiO_2$ Loading on $Na_2WO_4$-$TiO_2/SiO_2$

The $Na_2WO_4$-$TiO_2/SiO_2$ catalyst was further studied by varying the amount of $TiO_2$. In a previous study, 5wt% $Na_2WO_4$ loaded on $SiO_2$ using incipient-wetness impregnation was reported to produce an optimum yield for the OCM reaction [17]. However, the effect of $TiO_2$ loading on $Na_2WO_4/SiO_2$ has never been studied. In the present study, different amounts of $TiO_2$ on $Na_2WO_4/SiO_2$ were studied by varying the amounts of $TiO_2$ from 0 to 30% on the catalyst and keeping the amount of $Na_2WO_4$ on every catalyst unchanged at 5 wt%, as plotted in Fig. 2. As increasing $TiO_2$ loading, the $C_{2+}$ selectivities slowly increased from 38.0 to 44.9%, while the $CH_4$ conversion steadily decreased from 6.4 to 4.3%. Nevertheless, the $C_{2+}$ yield had an optimum yield at 5 wt% loading (2.7% $C_{2+}$ yield). This confirmed that the addition of $TiO_2$ into $Na_2WO_4/SiO_2$ enhances $C_{2+}$ formation. However, $TiO_2$ loadings over 5 wt% decreased the $C_{2+}$ yield of each catalyst. Thus, $Na_2WO_4$-$TiO_2/SiO_2$ catalyst at a total metal loading of 10 wt% and a $TiO_2$:$Na_2WO_4$ weight ratio of 1:1 (i.e. 5 wt% $Na_2WO_4$ + 5 wt% $TiO_2$) was chosen for the optimum catalyst for further studies.

### 3.3. Effect of $N_2/(4CH_4{:}1O_2)$ Feeding Gas Ratio and Reactor Temperature

The optimal catalyst was further investigated at various $N_2/(4CH_4{:}1O_2)$ feeding gas ratios ($N_2/(4CH_4{:}1O_2)$ = 0.0–1.5) and reactor temperatures (600–800 °C). For the previous studies in sections 3.1 and 3.2, the testing conditions were fixed at a $CH_4$:$O_2$ feeding gas ratio of 4:1 with a total feed flow rate of 50 mL/min (GHSV = 9,500 $h^{-1}$) without an inert gas at 700 °C and atmospheric pressure. In this section, $N_2$ gas (a diluent gas) was co-fed with $CH_4$:$O_2$ by fixing the volume ratio of $CH_4$:$O_2$ = 4:1 and varying the volume ratio of $N_2/CH_4$:$O_2$ from 0.0 to 1.5, and also varying the reactor temperature from 600 to 800 °C, while the

total feed flow rate was fixed at 50 mL/min. The $C_{2+}$ yield, $C_{2+}$ selectivity, and $CH_4$ conversion under each set of condition of the optimal catalyst are presented in Figs. 3(a), 3(b) and 3(c), respectively.

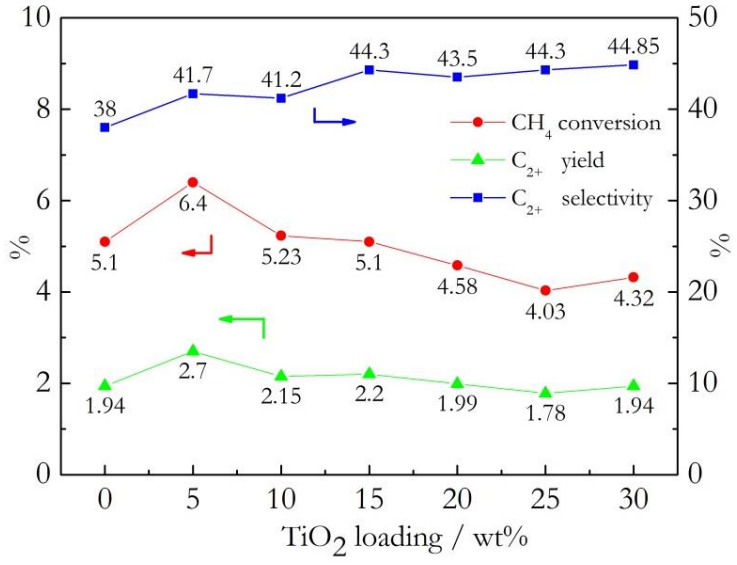


Fig. 2. $TiO_2$ loadings onto $Na_2WO_4/SiO_2$ from 0–30 wt% by fixing the amount of $Na_2WO_4$ onto each catalyst at 5 wt%; Testing conditions: feeding gas ratio of $CH_4$:$O_2$ = 4:1 by volume, total feed flow rate = 50 mL/min (GHSV = 9,500 $h^{-1}$), and reactor temperature = 700 °C.

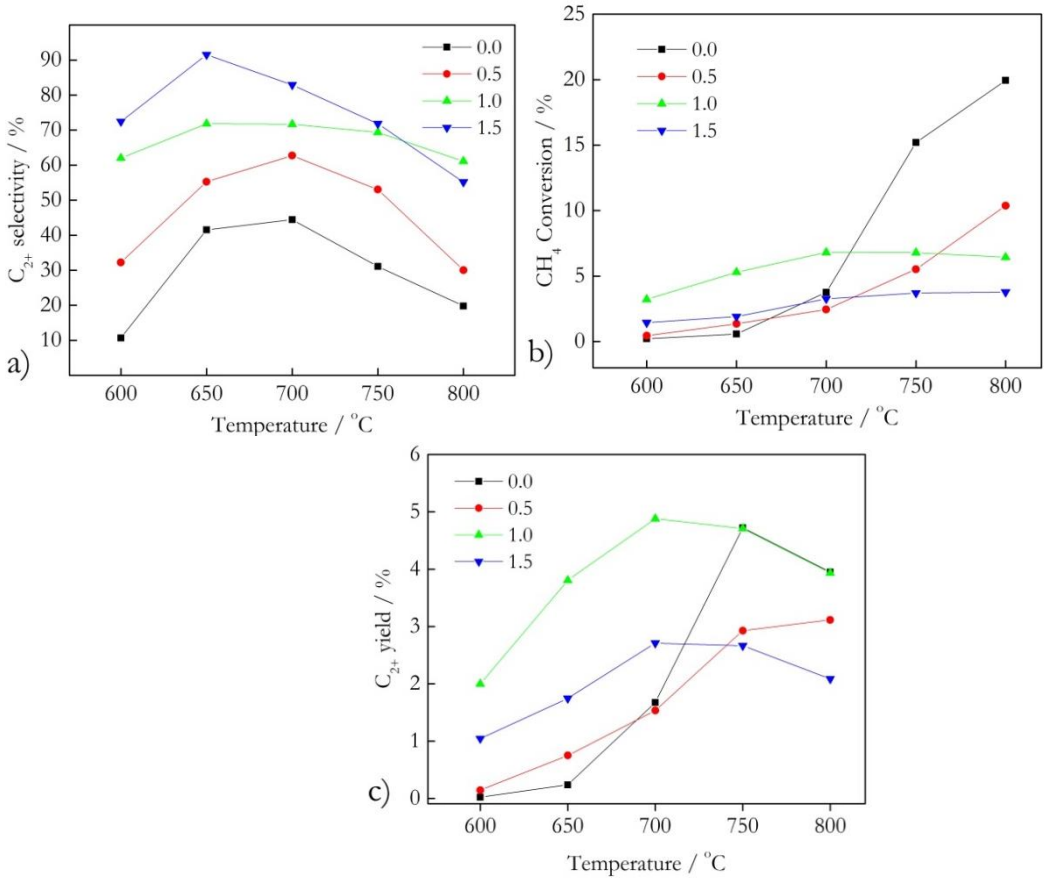


Fig. 3. a) $C_{2+}$ selectivity, b) $CH_4$ conversion, and c) $C_{2+}$ yield of the optimum $TiO_2$-$Na_2WO_4/SiO_2$ catalyst at $N_2/(4CH_4{:}1O_2)$ feeding gas ratios of 0.0–1.5 by volume, reactor temperatures of 600–800 °C, and total feed flow rate of 50 mL/min.

DOI:10.4186/ej.2019.23.5.169

Comparing the $C_{2+}$ selectivities at one reactor temperature (Fig. 3(a)), the $C_{2+}$ selectivity mostly increased as the $N_2/(4CH_4{:}1O_2)$ feeding gas ratio increased. The maximum $C_{2+}$ selectivity obtained was 91.5% with a $N_2/(4CH_4{:}1O_2)$ feeding gas ratio of 1.5 by volume and a reactor temperature of 650 ºC but the $CH_4$ conversion and the $C_{2+}$ yield were low at 1.9% and 1.7%, respectively. However, the $C_{2+}$ yield at every testing temperature decreased when the $N_2/(4CH_4{:}1O_2)$ feeding gas ratio was over 1.0 by volume because the reactant gases (i.e. $CH_4$ and $O_2$) were too diluted. In other words, the reactants were not sufficient for the active sites of the catalyst. In contrast, the $C_{2+}$ yield of the $N_2/(4CH4{:}1O_2)$ feeding gas ratio of 0.0 and 0.5 was lower than that of 1.0 because the reactant gases were much more than the active sites and the heat generated by the catalytic reaction in the catalyst's bed was high, so that the products can further combust in the hotspot zone. Thus, the $C_{2+}$ yields for these two conditions were relatively low.

Considering the catalytic activities at one $N_2/(4CH_4{:}1O_2)$ feeding gas ratio; the catalytic activities increased when the reactor temperatures was increased from 600 to 700 ºC. However, at reactor temperatures above 700 ºC, the $C_{2+}$ selectivities decreased with increasing $CH_4$ conversion, and thus the overall $C_{2+}$ production (i.e. $C_{2+}$ yields) decreased because the combustion of $CH_4$ to $CO_x$ products is favored at high reaction temperature [3], as well as the $C_{2+}$ products being able to further react with some active species of the catalyst or to react with $O_2$ gas in the gas phase to further produce $CO_x$ [18]. As seen in Fig. 3(c), the optimal $C_{2+}$ yield was achieved at 4.9% with 71.7% $C_{2+}$ selectivity and 6.8% $CH_4$ conversion when the operating conditions were an $N_2/(CH_4{:}O_2)$ feed gas ratio of 1.0 by volume and 700 ºC. These conditions were then chosen for a further study on the stability of the catalyst.

### 3.4. Catalytic Stability of $Na_2WO_4$-$TiO_2/SiO_2$

The catalytic stability of the $Na_2WO_4$-$TiO_2/SiO_2$ catalyst was investigated under the optimal conditions found in section 3.3. The activities of the catalyst over 24 h are presented in Fig. 4. Promisingly, the $C_{2+}$ selectivities were high at approximately 69–71% during the testing period. However, the overall selectivity reduced by approximately 3% within 24 h. Moreover, the $CH_4$ conversions slowly decreased from 6.8 to 5.9, leading to decreased $C_{2+}$ yield during the test period. It was also noticed that the $CO_x$ selectivities gradually increased from 29 to 31%. The results suggested that the stability of the $Na_2WO_4$-$TiO_2/SiO_2$ catalyst was quite good for over 24 h. The slow deactivation of the catalyst requires further study, which is not the focus of this report.

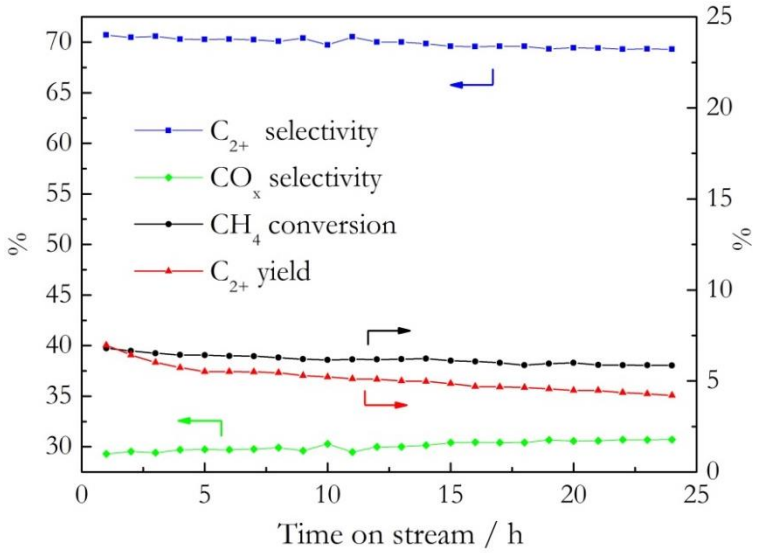


Fig. 4. Catalytic performance of $Na_2WO_4$-$TiO_2/SiO_2$ catalyst, testing conditions: $N_2/(4CH_4{:}1O_2)$ feeding gas ratio of 1.0, reactor temperature of 700 ºC, total feed flow rate of 50 mL/min, atmospheric pressure, and 24 h of testing.

### 3.5. Characterization of $TiO_2/SiO_2$, $Na_2WO_4/SiO_2$, and $Na_2WO_4$-$TiO_2/SiO_2$ Catalysts

The XRD pattern of the $Na_2WO_4$-$TiO_2/SiO_2$ catalysts compared with that of the $TiO_2/SiO_2$ and $Na_2WO_4/SiO_2$ catalysts are presented in Fig. 5. The $TiO_2/SiO_2$ catalyst exhibited two small peaks at $2\theta$ of 25.2 and 48.5, indicating the presence of crystalline $TiO_2$ (anatase). It was also noticed that the $SiO_2$ support was in the amorphous phase. For the $Na_2WO_4/SiO_2$ catalyst, two crystalline compounds were observed. The first one was the crystalline $Na_2WO_4$, showing the characteristic peaks at $2\theta$ of 7.16, 27.5, 32.4 and 48.4. The other was the presence of α-cristobalite (one of the crystalline forms of $SiO_2$), exhibiting the characteristic peaks at $2\theta$ of 21.9, 28.3, 31.3, 36.0, 47.8, and 56.9. It was surprising to observe the formation of α-cristobalite at low a calcination temperature (800 ºC) in the presence of $Na_2WO_4$ because this crystalline form of $SiO_2$ normally occurs at calcination temperatures above 1,500 ºC [19]. Similarly, the α-cristobalite phase was observed in the $Na_2WO_4$-$TiO_2/SiO_2$ catalyst as clearly indicated by the characteristic XRD pattern. It was more interesting to observe that the characteristic peaks of $TiO_2$ were clearly seen for the $Na_2WO_4$-$TiO_2/SiO_2$ catalyst compared to those peaks in the $Na_2WO_4$-$TiO_2/SiO_2$ catalyst. This suggested that the environment in this catalyst enhanced the crystallinity of $TiO_2$. Thus, the important factor that promotes the formation of $C_{2+}$ products of the $Na_2WO_4$-$TiO_2/SiO_2$ catalyst was the formation of the crystalline components (α-cristobalite, $Na_2WO_4$, and $TiO_2$).

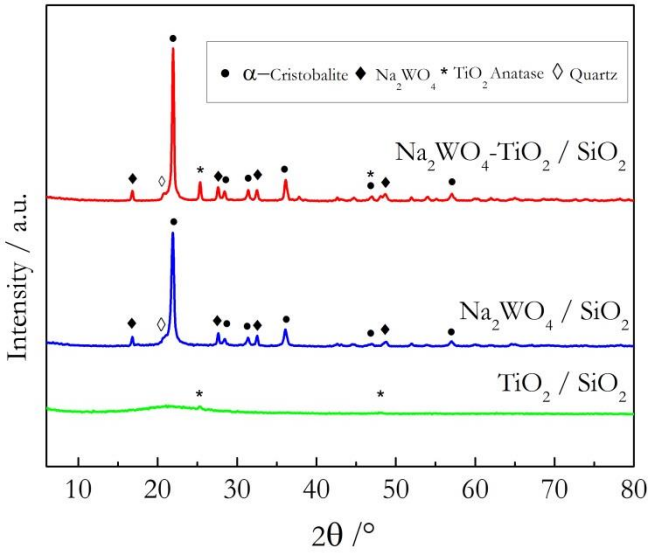


Fig. 5. XRD patterns of $TiO_2/SiO_2$, $Na_2WO_4$ /$SiO_2$, and $Na_2WO_4$-$TiO_2/SiO_2$.

The surface morphologies of the three catalysts imaged using FE-SEM were compared with the pure $SiO_2$ support and these are illustrated in Fig. 6(a)–Fig. 6(f). The $SiO_2$ support (Fig. 6(a)) and the $TiO_2/SiO_2$ catalyst (Fig. 6(b)) are similar, in that the particles are irregular in shape with sizes ranging from 20 to 50 nm. These particles were observed mostly in the amorphous $SiO_2$ support. The particles of the $Na_2WO_4/SiO_2$ catalyst (Fig. 6(c) and Fig. 6(d)) were also irregular in shape. Interestingly, the typical shape of the amorphous $SiO_2$ was completely transformed to a new shape, which was larger in size and possessed coral-reef like structures (approximately > 0.5 μm in diameter). This new structure was the crystalline α-cristobalite as identified by the XRD pattern. The $Na_2WO_4$-$TiO_2/SiO_2$ catalyst (Fig. 6(e) and Fig. 6(f) had similar the size and shape to the particles of the $Na_2WO_4/SiO_2$ catalyst. However, some small particles (approximately 50-100 nm in diameter) were observed throughout the catalyst. These particles were identified as $TiO_2$ crystals.

The TEM images of the $Na_2WO_4$-$TiO_2/SiO_2$ catalyst compared with those of the $TiO_2/SiO_2$ and $Na_2WO_4/SiO_2$ catalysts are shown in Fig. 7. The shape and size of each catalyst corresponded to the observation in the FE-SEM images (Fig. 6). The TEM images of the $Na_2WO_4/SiO_2$ (Fig. 7(c) and 7(d)) and $Na_2WO_4$-$TiO_2/SiO_2$ (Fig. 7(e) and 7(f)) catalysts confirmed that the amorphous $SiO_2$ support transformed to α-cristobalite when adding $Na_2WO_4$, in agreement with a previous report [20]. For the $Na_2WO_4$-

DOI:10.4186/ej.2019.23.5.169

$TiO_2/SiO_2$ catalyst, crystalline $TiO_2$ particles were clearly observed with sizes ranging between 50 and 100 nm.

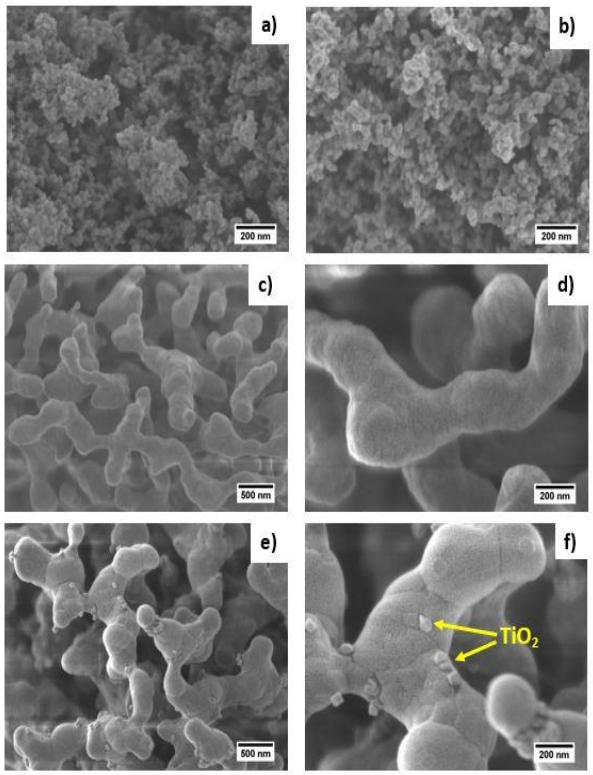


Fig. 6. SEM images of pure $SiO_2$ support (a), $TiO_2/SiO_2$ (b), $Na_2WO_4/SiO_2$ (c, d), and $Na_2WO_4$-$TiO_2/SiO_2$ (e, f).

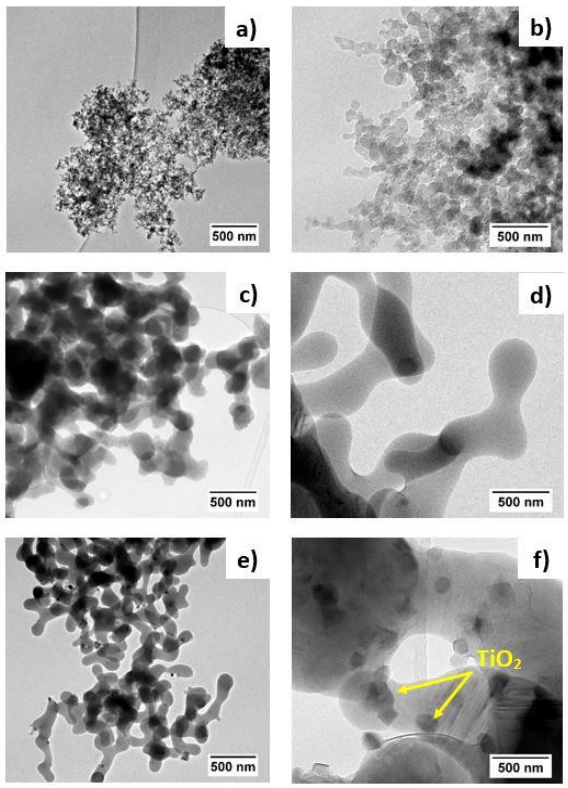


Fig. 7. TEM images of $TiO_2/SiO_2$ (a, b), $Na_2WO_4/SiO_2$ (c, d), and $Na_2WO_4$-$TiO_2/SiO_2$ (e, f).

The BET surface areas, pore sizes, and pore volumes of the catalysts were measured using an $N_2$-sorption analyzer. For comparison, the commercial $SiO_2$ support (surface area of 85–115 $m^2/g$, amorphous fumed silica, Alfa Aesar) was also dried and calcined using the same method as the catalyst preparation without adding any metal precursors and conducting the BET measurement. As presented in Table 1 and Fig. 8, the isotherm plot of the $SiO_2$ support was similar to that of the $TiO_2/SiO_2$ catalyst, in which no hysteretic loop was observed. This indicated that the $SiO_2$ support and the $TiO_2/SiO_2$ catalyst are non-porous material, and thus their porous sizes and volumes must have been created from the inter-particles. However, the surface area of the $SiO_2$ support was lower than that of the $TiO_2/SiO_2$ catalyst, suggesting that the $TiO_2$ particles potentially deposited on the surface of $SiO_2$ and create new surfaces, and thus the surface area of the $TiO_2/SiO_2$ catalyst increased. The surface areas of the $Na_2WO_4/SiO_2$ and $Na_2WO_4$-$TiO_2/SiO_2$ catalysts were much lower than those of the $SiO_2$ support and the $TiO_2/SiO_2$ catalyst. This was consistent with the observations from using the FE-SEM (Fig. 6.) & TEM (Fig. 7.) images, in which the particle sizes of the catalysts containing $Na_2WO_4$ were larger than those of the $TiO_2$ catalyst. The hysteretic loops of the $Na_2WO_4/SiO_2$ and $Na_2WO_4$-$TiO_2/SiO_2$ catalysts were similar, in which the pore sizes and the pore volumes generated from the intra-particles and the pore sizes were classified as a meso-porous material. Although the $Na_2WO_4$-$TiO_2/SiO_2$ catalyst had a quite small specific surface area, this catalyst had the highest $C_{2+}$ yield, indicating that the synergistic catalyst effect or the selected active components plays a significant role in the catalytic performance.

Table 1. BET surface area (S.A.), pore size, and pore volume of $TiO_2/SiO_2$, $Na_2WO_4/SiO_2$, and $Na_2WO_4$-$TiO_2/SiO_2$ compared with pure $SiO_2$ support.

| Material | S.A. ($m^2/g$) | Pore size (nm) | Pore volume ($cm^3/g$) |
|---|---|---|---|
| $SiO_2$ | 86.5 | 22.2 | 0.480 |
| $Na_2WO_4$ / $SiO_2$ | 6.5 | 9.1 | 0.015 |
| $TiO_2$ / $SiO_2$ | 106.2 | 17.5 | 0.460 |
| $Na_2WO_4$-$TiO_2$/ $SiO_2$ | 5.4 | 10.0 | 0.013 |

The FT-IR patterns of the catalysts are presented in Fig. 9. All three catalysts displayed the Si—O—Si rocking, the Si—O—Si bending, and the Si—O—Si stretching peaks appearing around 490, 800, and 1100 $cm^{-1}$, respectively. There was one different peak appearing at 621 $cm^{-1}$ for $Na_2WO_4$-$TiO_2/SiO_2$ and $Na_2WO_4/SiO_2$, specifying the existence of α-cristobalite [19] in these two catalysts, in good agreement with the findings in Fig. 5. As can be seen by the catalyst activities presented in Fig. 1, the $Na_2WO_4$-$TiO_2/SiO_2$ catalyst had a $C_{2+}$ yield greater than those of the two single catalysts. Thus, one of the important keys that can be considered to improve the $C_{2+}$ yield is to have a catalyst consisting of α-cristobalite interacting with an active crystalline metal oxide.

DOI:10.4186/ej.2019.23.5.169

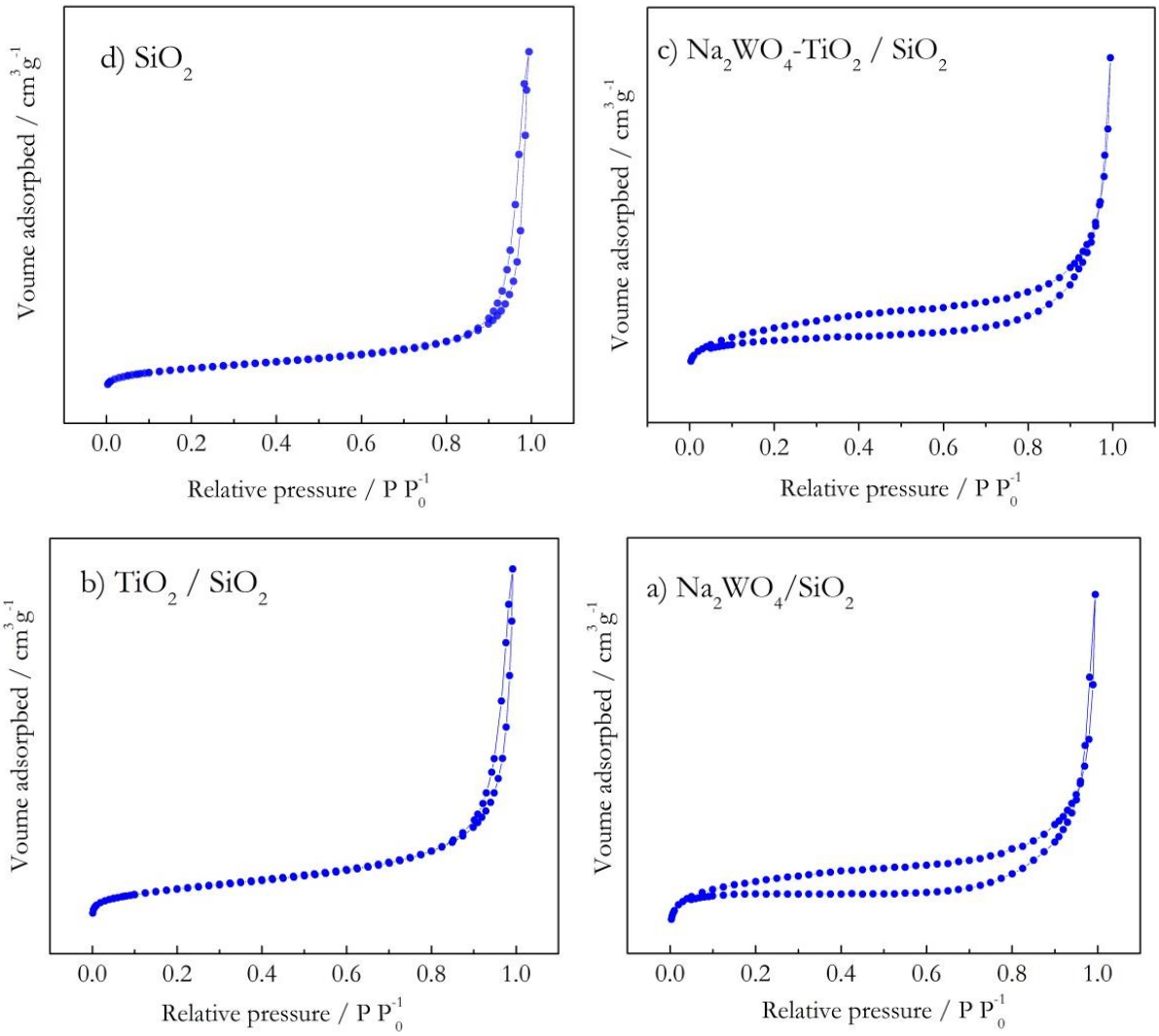


Fig. 8. Isotherm plots of (a) $Na_2WO_4/SiO_2$ catalyst, (b) $TiO_2/SiO_2$ catalyst, (c) $Na_2WO_4$-$TiO_2/SiO_2$ catalyst, and (d) pure $SiO_2$ support.

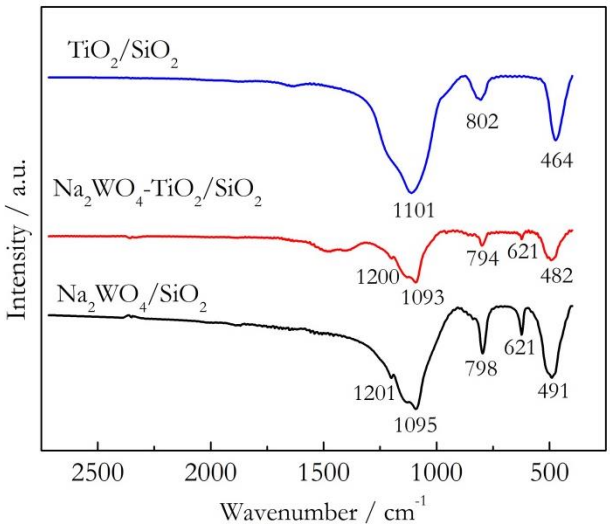


Fig. 9. FT-IR spectra of $Na_2WO_4$-$Ti/SiO_2$, $Na_2WO_4/SiO_2$, and $TiO_2/SiO_2$ catalysts.

Figure 10 presents the XPS spectra of the catalysts. The XPS scans were carried out in the range of the Na, W, and Ti regions. The observed peaks corresponded to $Na_2O$ (1s = 1071.5 eV) $WO_4^{2-}$($4f_{5/2}$ = 37.6 eV, $4f_{7/2}$ = 35.3 eV ) for $Na_2WO_4/SiO_2$ and ($4f_{5/2}$ = 37.8 eV, $4f_{7/2}$ = 35.3 eV) for $Na_2WO_4$-$TiO_2/SiO_2$, and $TiO_2$ ($2p_{3/2}$ = 464.2 eV, $2p_{1/2}$ = 459.2 eV) for $TiO_2/SiO_2$ and ($2p_{3/2}$ = 464.5 eV, $2p_{1/2}$ = 458.8 eV) for $Na_2WO_4$-$TiO_2/SiO_2$. Of interest was that the peaks of $WO_4^{2-}$and $TiO_2$ shifted toward a higher binding energy when $Na_2WO_4$ and $TiO_2$ were present in the same catalyst. This was because the Ti or W species are more likely to attach to $WO_4^{-2}$ or $O^{2-}$ bonding with Ti, which is an electron withdrawing group. Thus, the oxidation state of Ti or W has a higher positive charge, and thus shifts in the binding energies can be observed.

Catalyst reducibility and the interaction between the active catalysts and the support were examined using the $H_2$-TPR technique (see Fig. 11). For the $TiO_2/SiO_2$ catalyst, no clear $H_2$ reduction peak could be seen in this temperature range, consistent with previous reports [21, 22]. For $Na_2WO_4/SiO_2$, a broad reduction peak starting from 450 ºC to above 900 ºC with a maximum $H_2$ consumption at about 800 ºC was observed, indicating the reduction of W species [22]. The reduction behavior of the $Na_2WO_4$-$TiO_2/SiO_2$ catalyst was related to that of the $Na_2WO_4/SiO_2$ catalyst. However, the starting reduction temperature and the maximum temperature of the $Na_2WO_4$-$TiO_2/SiO_2$ catalyst shifted toward a higher temperature (approximately 50 ºC greater than those of the $Na_2WO_4/SiO_2$ catalyst). This suggested that the redox properties of these metal species substantially change, probably because there is a strong interaction between the $WO_4^{2-}$ component and the $TiO_2$ crystals [22].

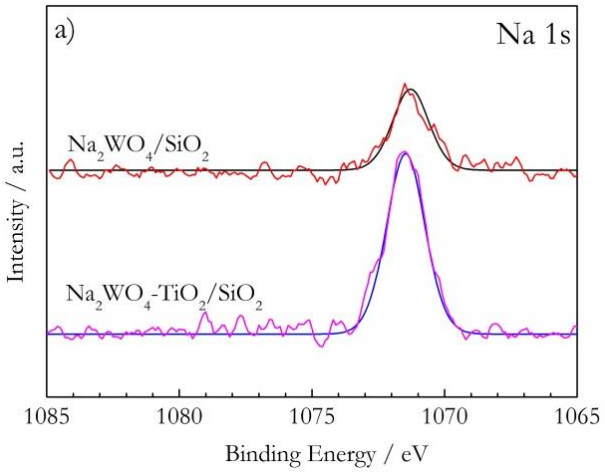


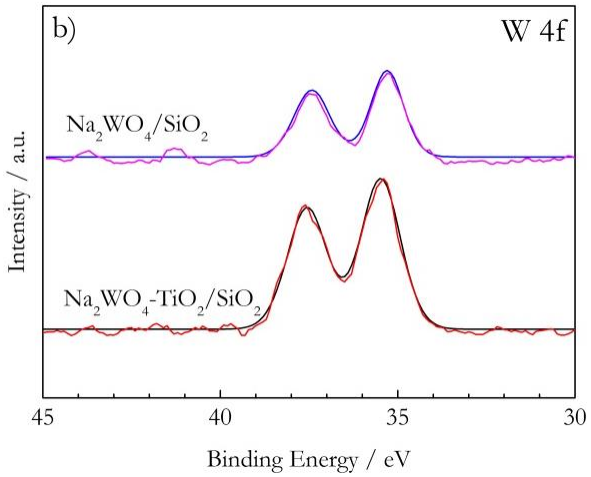

DOI:10.4186/ej.2019.23.5.169

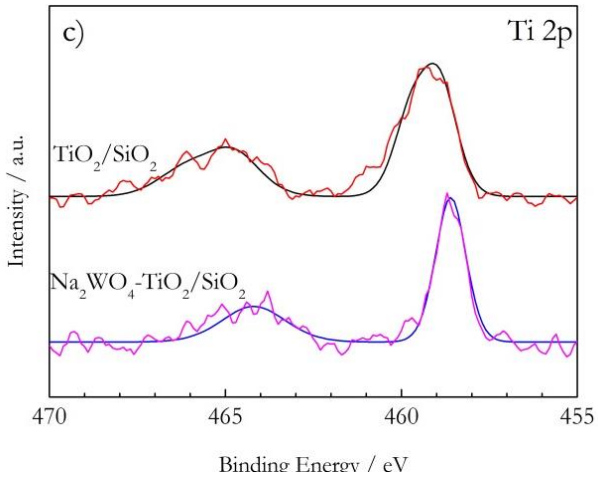


Fig. 10. XPS spectra of $Na_2WO_4$-Ti/$SiO_2$, $Na_2WO_4/SiO_2$, and $TiO_2$ /$SiO_2$ showing scanning in the (a) Na, (b) W, and (c) Ti ranges.

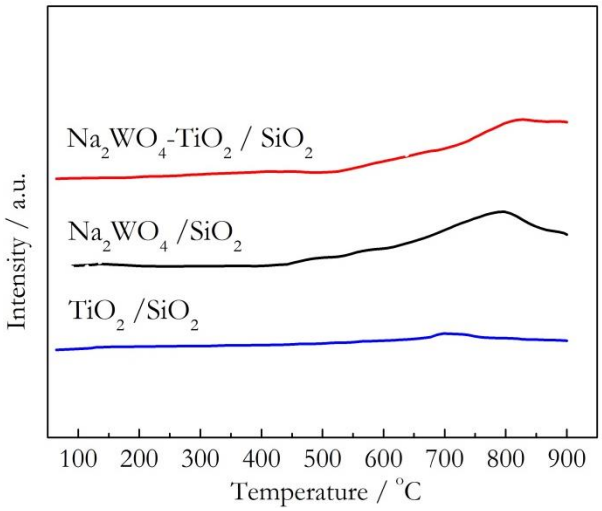


Fig. 11. $H_2$-TPR patterns of $Na_2WO_4$-$TiO_2/SiO_2$, $Na_2WO_4$/ $SiO_2$, and $TiO_2/SiO_2$.

In previous reports on the activity of catalysts containing $Na_2WO_4$ and $SiO_2$ for OCM reaction, there have been some suggestions about the enhancement of those catalysts as follows. Ji, et al. stated that the existence of the α-cristobalite phase was a critical necessity for the $C_{2+}$ formation of catalysts containing $Na_2WO_4$ and $SiO_2$ for OCM reaction [9]. Elkins, et al. claimed that the interaction between the α-cristobalite structure and the $WO_4^{2-}$ tetrahedron structure was crucial in the generation of $C_{2+}$ and the inter-phase between these two components was the active surface species. Moreover, the $WO_4^{2-}$ tetrahedron could stabilize the $Mn_2O_3$ and $Na_2WO_4$ phases, so that the catalysts could maintain their high activity during the reaction [23]. Furthermore, Palermo, et al. suggested that Na played dual roles in promoting the activity of $MnO_x$-$Na_2WO_4/SiO_2$ catalysts by acting as both a chemical and a structural promoter [24, 25]. From these reports, it can be certainly claimed that the presence of the α-cristobalite structure, the crystalline $Na_2WO_4$, and the anatase-$TiO_2$ crystals in the $Na_2WO_4$-$TiO_2/SiO_2$ catalyst strongly enhances the activity of the catalyst and is crucial for the formation of $C_{2+}$ in the reaction.

## 4. Conclusions

The combination of 5wt% $TiO_2$ and 5wt% $Na_2WO_4$ on $SiO_2$ support (i.e. $Na_2WO_4$-$TiO_2$), prepared using the co-impregnation method, was superior to the single catalysts of its component (i.e. $Na_2WO_4/SiO_2$, $TiO_2/SiO_2$). In studying the operating conditions by co-feeding $N_2$ gas as a diluent gas into the reactant

gases at different volume ratios and different temperatures, the maximum $C_{2+}$ yield was found at an $N_2/(4CH_4{:}1O_2)$ feeding gas ratio 1:1 by volume and at 700 ºC. The $Na_2WO_4$-$TiO_2$ catalyst produced the highest $C_{2+}$ yield at 4.9% with 71.7% $C_{2+}$ selectivity and 6.8% $CH_4$ conversion under these optimal operating conditions. Furthermore, the activity of the catalyst had good stability over 24 h of testing. Characterization of the $Na_2WO_4$-$TiO_2$ catalyst using XRD and FT-IR showed that α-cristobalite and crystalline anatase-$TiO_2$ were present. These two crystal components played a significant role in the formation of $C_{2+}$ for the OCM reaction. The FE-SEM, TEM, and BET results were in good agreement with the findings of the XRD and FT-IR analyses. Of great interest for future study is the analysis of the kinetic mechanism of the catalyst for OCM reaction or improvement of the catalyst activity by adding promoters.

## Acknowledgements

We would like to thanks the Thailand Research Fund and the Commission on Higher Education (grant numbers IRG5980004 & MRG6180232); the National Nanotechnology Center (NANOTEC), NSTDA, Ministry of Science and Technology, Thailand, through its program of Research Network NANOTEC (RNN); the Center of Excellence on Petrochemical and Materials Technology; the Kasetsart University Research and Development Institute (KURDI); and the Department of Chemical Engineering and the Faculty of Engineering at Kasetsart University for financial supports. P. Kidamorn received funding through a scholarship from the Faculty of Engineering at Kasetsart University.

## References

[1] G. J. Hutchings, M. S. Scurrell, and J. R. Woodhouse, "Oxidative coupling of methane using oxide catalyst," *Chem. Soc. Rev.*, vol. 18, pp. 251-283, 1989.

[2] M. Y. Sinev, Z. T. Fattakhova, V. I. Lomonosov, and Y. A. Fordienko, "Kinetics of oxidative coupling of methane: bridging the gap between comprehension and description," *J. Nat. Gas Chem.*, vol. 18, pp. 273-287, 2009.

[3] K. Khammona, S. Assabumrungrat, and W. Wiyarath, "Reviews on coupling of methane over catalysts for application in $C_2$ hydrocarbon production," *J. Eng. Appl. Sci.*, vol. 7, pp. 447-455, 2012.

[4] S. M. K. Shahri and A. N. Pour, "Ce-promoted Mn/$Na_2WO_4$/$SiO_2$ catalyst for oxidative coupling of methane at atmospheric pressure," *J. Nat. Gas Chem*, vol. 19, pp. 47-53, 2010.

[5] R. Mariscal, M. A. Pena, and J. L. G. Fierro, "Promoter effects of dichloromethane on the oxidative coupling of methane over MnMgO catalysts," *Appl. Catal., A*, vol. 131, pp. 243-261, 1995.

[6] V. R. Choudhary, V. H. Rane, and S. T. Chaudhari, "Factors influencing activity/selectivity of La-promoted MgO catalyst prepared from La- and Mg- acetates for oxidative coupling of methane," *Fuel*, vol. 79, pp. 1487-1491, 2000.

[7] Z. Gholipour, A. Malekzadeh, R. Hatami, Y. Mortazavi, and A. Khodadadi,"Oxidative coupling of methane over ($Na_2WO_4$+Mn or Ce)/$SiO_2$ catalysts: In situ measurement of electrical conductivity," *J. Nat. Gas Chem*, vol. 19, pp. 35-42, 2010.

[8] R. T. Yunarti, M. Lee, Y. J. Hwang, D. J. Suh, J. Lee, I. W. Kim, and J. M. Ha, "Transition metal-doped $TiO_2$ nanowire catalysts for the oxidative coupling of methane," *Catal. Commun*, vol. 50, pp. 54-58, 2014.

[9] S. Ji, T. Xiao, S. Li, L. Chou, B. Zhang, C. Xu, R. Hou, A. P. E. York, and M. L. H Green, "Surface $WO_4$ tetrahedron: The essence of the oxidative coupling of methane over M-W-Mn/$SiO_2$ catalysts," *J. Catal.*, vol. 220, pp. 47-56, 2003.

[10] J. Y. Lee, W. Jeon, J. W. Choi, Y. W. Suh, J. M. Ha, D. J. Suh, and Y. K. Park, "Scaled-up production of $C_2$ hydrocarbons by the oxidative coupling of methane over pelletized $Na_2WO_4$/Mn/$SiO_2$ catalysts: Observing hot spots for the selective process," *Fuel.*, vol. 106, pp. 851-857, 2013.

[11] A. Malekzadeh, A. Khodadadi, A. K. Dalai, and M. Abedini, "Oxidative coupling of methane over Lithium doped (Mn+W)/$SiO_2$ catalysts," *J. Nat. Gas Chem*, vol. 16, pp. 121-129, 2007.

[12] J. Wang, L. Chou, B. Zhang, H. Song, J. Zhao, J. Yang, and S. Li, "Comparative study on oxidation of methane to ethane and ethylene over $Na_2WO_4$-Mn/$SiO_2$ catalysts prepared by different methods," *J. Mol. Catal. Chem.*, vol. 245, pp. 272-277, 2006.

[13] N. Hiyoshi and T. Ikeda, "Oxidative coupling of methane over alkali chloride-Mn-$Na_2WO_4/SiO_2$ catalysts: Promoting effect of molten alkali chloride," *Fuel Process. Technol.,* vol. 133, pp. 29-34, 2015.
[14] T. W. Elkins and H. E. Hagelin-Weaver, "Characterization of Mn-$Na_2WO_4/SiO_2$ and Mn-$Na_2WO_4$/MgO catalysts for the oxidative coupling of methane," *Appl. Catal., A*, vol. 497, pp. 96-106, 2015.
[15] F. Papa, D. Gingasu, L. Patron, A. Miyazaki, and I. Balint, "On the nature of active sites and catalytic activity for OCM reaction of alkaline-earth oxides-neodymia catalytic systems," *Appl. Catal., A,* vol. 375, pp. 172-178, 2010.
[16] V. H. Rane, S. T. Chaudhari, and V. R. Choudhary, "Oxidative coupling of methane over La-promoted CaO catalysts: Influence of precursors and catalyst preparation method," *J. Nat. Gas Chem.*, vol. 19, pp. 25-30, 2010.
[17] D. J. Wang, M. P. Rosynek, and J. H. Lunsford, "Oxidative coupling of methane over oxide-supported sodium-manganese catalysts," *J. Catal.*, vol. 155, pp. 390-402, 1995.
[18] F. Basile, G. Fornasari, F. Trifiro, and A. Vaccari, "Partial oxidation of methane: Effect of reaction parameters and catalyst composition on the thermal profile and heat distribution," *Catal. Today*, vol. 64, pp. 21-30, 2001.
[19] S. Ji, T. Xiao, S. Li, L. Chou, B. Zhang, C. Xu, R. Hou, A. P. E York, and M. L. H Green, "Surface $WO_4$ tetrahedron: the essence of the oxidative coupling of methane over M·W·Mn/$SiO_2$ catalysts," *J. Catal.*, vol. 220, pp. 47-56, 2003.
[20] A. M. Venezia, F. Raimondi, V. La Parola, and G. Deganello, "Influence of sodium on the structure and HDS activity of Co-Mo catalysts supported on silica and aluminosilicate," *J. Catal.*, vol. 194, pp. 393-400, 2000.
[21] T. Chukeaw, A. Seubsai, P. Phon-in, K. Charoen, T. Witoon, W. Donphai, P. Parpainainar, M. Chareonpanich, D. Noon, B. Zohour, and S. Senkan, "Multimetallic catalysts of $RuO_2$–CuO–$Cs_2O$–$TiO_2/SiO_2$ for direct gas-phase epoxidation of propylene to propylene oxide," *RSC Adv.*, vol. 6, pp. 56116-56126, 2016.
[22] J. Li, G. Lu, G. Wu, D. Mao, Y. Guo, Y. Wang, and Y.Guo, "Effect of $TiO_2$ crystal structure on the catalytic performance of $Co_3O_4/TiO_2$ catalyst for low-temperature CO oxidation," *Catal. Sci. Technol.*, vol. 4, pp. 1268-1275, 2014.
[23] T. W. Elkins, and H. E. Hagelin-Weaver, "Characterization of Mn-$Na_2WO_4/SiO_2$ and Mn-$Na_2WO_4$/MgO catalysts for the oxidative coupling of methane," *Appl. Catal., A*, vol. 497, pp. 96-106, 2015.
[24] A. Palermo, J. P. H Vazquez, A. F. Lee, M. S. Tikhov, and R. M. Lambert, "Critical influence of the amorphous silica-to-cristobalite phase transition on the performance of Mn/$Na_2WO_4/SiO_2$ catalysts for the oxidative coupling of methane," *J. Catal.*, vol. 177, pp. 259-266, 1998.
[25] Y. T. Chua, A. R. Mohamed, and S. Bhatia, "Oxidative coupling of methane for the production of ethylene over sodium-tungsten-manganese-supported-silica catalyst (Na-W-Mn/$SiO_2$)," *Appl. Catal., A*, vol. 343, pp. 142-148, 2008.